

A physics-based micromechanical model for electroactive viscoelastic polymers

Roberto Brighenti¹ , Andreas Menzel^{2,3} and Franck J Vernerey⁴

Journal of Intelligent Material Systems and Structures

2018, Vol. 29(14) 2902–2918

© The Author(s) 2018

Article reuse guidelines:

sagepub.com/journals-permissions

DOI: 10.1177/1045389X18781036

journals.sagepub.com/home/jim



Abstract

Electroactive polymers with time-dependent behavior are considered in the present paper by way of a new physics-based micromechanical model; such viscoelastic response is described by the internal evolution of the polymer network, providing a new viewpoint on the stress relaxation occurring in elastomers. The main peculiarity of such internally rearranging materials is their capacity to locally reset their reference stress-free state, leading to a mechanical behavior that relaxes out (eases off) an induced stress state and that can thus be assimilated to a sort of internal self-healing process. Such high deformability and recoverability displayed by dynamically cross-linked polymers can be conveniently exploited when they are coupled in electromechanical problems; the deformation induced by an electric field can be easily tuned by the intensity of the electric field itself and the obtained shape can be maintained without any electric influence once the material microstructure has rearranged after a sufficient curing time. In the present paper, both features of the polymeric material, that is, internal remodeling and electromechanical coupled response, are considered and a theoretical framework is established to simulate representative boundary value problems.

Keywords

Electroactive polymers, electromechanical coupling, cross-link evolution, morphing

Introduction

The description of the mechanical response of highly deformable polymers, involves a number of physical phenomena at the molecular level that include complex interaction of elastic, viscous flow, and partially reversible deformation. The elastic fraction of the mechanical behavior derives from the stretch of the polymer chains network, typical for this class of amorphous materials, while irreversible or partially irreversible phenomena are induced by several mechanisms occurring at the molecular level, such as chain sliding, loss of chain bonds, and chain unentanglement. The picture outlined above becomes even more complex by considering that some other factors can influence the mechanical response such as the temperature, the presence of a solvent phase (that occurs in the case of gels), mechanisms influenced by loading time rate (Doi, 2013; Flory, 1953, 1989; Kuhn and Gr \ddot{u} n, 1946; Orlandini and Whittington, 2016; Treloar, 1975), etc.

Polymeric materials are often characterized by a highly rate-dependent response and hysteretic behavior upon cyclic loading (Bergstr \ddot{o} m and Boyce, 2016; Lavoie et al., 2016; Petiteau et al., 2013; Roland, 2006). It has been also discovered that some polymers, such as

the natural rubbers—if strongly stretched at room temperature—present a strain-induced crystallization that enhances switching their microstructure from amorphous to a semicrystalline-like one thanks to the development of a clearly oriented microstructure arising parallel to the tensile direction (Candau et al., 2014). At the molecular level, the structure of polymers is fully amorphous and consists of a three-dimensional network of long linear entangled chains linked together at several discrete points termed as cross-links; the mechanical properties of polymeric materials are strongly related to relative motion and interaction between their chains, but most of all to the volume

¹Department of Engineering and Architecture, University of Parma, Parma, Italy

²Institute of Mechanics, TU Dortmund, Dortmund, Germany

³Division of Solid Mechanics, Lund University, Lund, Sweden

⁴Department of Mechanical Engineering, University of Colorado Boulder, Boulder, CO, USA

Corresponding author:

Roberto Brighenti, Department of Engineering and Architecture, University of Parma, Viale delle Scienze 181A, 43124 Parma, Italy.
Email: brigh@unipr.it

density of such bonds, rather than to the molecular structure of the chains themselves.

On the other hand, the intensity of the strength existing between atoms in traditional crystalline materials is responsible for their mechanical characteristics while the entropy-related effects are negligible in such a class of materials. However, the mechanical deformation occurring in amorphous elastomers cannot be quantified without accounting for the entropic nature of the deformation that usually involves a strong geometrical rearrangement and chain reordering with the consequence to decrease the system's entropy.

The above mentioned chain reorganization and their relative interaction can also be invoked to physically explain, from a micromechanics point of view, the time-dependent behavior shown by polymers. Slow unentanglement usually takes place under mechanical stretch and is responsible for their viscoelastic behavior; upon unloading, the initial stress-free and strain-free state is often recovered and the viscous effects can thus be seen as phenomena inducing a time delay in the mechanical response. In the present paper, we model the above described time-dependent phenomena through an extension of the classic statistics-based approach to the mechanics of elastomers by quantifying the evolution of the material's network structure in time.

Typically, the mechanical behavior of polymers is modeled based on the deformation mechanism of their microstructure which is described using a statistical approach; the distribution function of the polymeric chains' end-to-end vectors is quantitatively given by several statistical parameters (such as mean value, dispersion) and can be related to the mechanical properties of the material itself (Doi, 2013; Flory, 1953, 1989; Treloar, 1975).

A proper description of the time evolution of such a distribution function provides a simple and effective way to quantify the macroscopic behavior of polymers on the basis of their micromechanical features; the reorganization of the polymer network in time—depending on the load intensity, load rate, and chemo-physics of internal chains evolution (Brighenti and Vernerey, 2017; Drozdov, 1999; Fricker, 1973; Meng et al., 2016; Yang et al., 2015)—if properly calibrated, can lead to a precise quantification of the time-related phenomena and represents a convenient alternative to more classic approaches. Polymeric materials characterized by dynamic covalent cross-links have been recently developed and are nowadays known as vitrimers (Jurewska and Jurewski, 2015; Smullenburg et al., 2013); they possess the strength of thermoset materials as well as the forming capability of thermoplastic polymers when the bond exchange is triggered by a sufficient thermal energy supply.

As a matter of fact, standard methods for the study of the macroscopic mechanical response of polymers are usually based on the description of the physical

states of polymer chains in an average fashion, such as the use of differential or integral viscoelastic models (Osswald and Rudolph, 2014), and the multiplicative decomposition of the deformation gradient tensor to account for dissipative and inelastic phenomena, leading to viscous-related terms in the expression of the free energy (Ask et al., 2012a).

The internal reorganization in time of the material during the loading process leads to the fact that the existence of a unique reference state—with respect to which the deformation has to be measured—cannot easily be identified. From this point of view, a polymeric material that continuously reorganizes its microstructure in time can be modeled as a non-Newtonian fluid, whose response is usually sensitive to the deformation rate and, partially, to the total deformation experienced; classic formulations in such a context are represented by the linear Maxwell and Kelvin–Voigt models or the Oldroyd-B model (Oldroyd, 1950).

The evident compliance shown by elastomeric polymers has attracted the attention of many researchers in recent years who used such materials as sensors or actuators by coupling them with an electrical field (Bustamante et al., 2008, 2009; Dorfmann and Ogden, 2005; Rasmussen, 2012; Tiersten, 1971; Toupin, 1956); because of their capability to display large deformation under the application of an electrical potential, such electromechanical coupling leads to the so-called smart materials systems thanks to their ability to suddenly deform under external non-mechanical stimuli. Seen from this position, they provide an effective tool to develop advanced mechanical applications such as artificial muscles, soft actuators, sensors, biomedical devices (Tagarielli et al., 2012; Wissler and Mazza, 2007). On the other hand, the physical coupling between mechanical response and electric field (Dorfmann and Ogden, 2012) is usually quantitatively considerable and highly nonlinear, and suitable theoretical approaches have been proposed and developed so far to face such a problem (Ask et al., 2012b; Büschel et al., 2013; Cohen et al., 2016; Thylander et al., 2017). Furthermore, it is worth mentioning that the development in recent years of highly deformable and polarizable materials has increased the attention even more on this class of materials, opening the door to new and unprecedented applications (Dorfmann and Ogden, 2014; Haldar et al., 2016; Menzel and Waffenschmidt, 2009).

As mentioned above, a precise and quantitative description of the mesoscopic response, obtained on the basis of the mechanisms occurring in the material at the microscale, requires a correct understanding of the involved phenomena and the formulation of a suitable model to describe how the evolving chemically and physically driven polymer microstructure modification reflects in its behavior observable at the continuum level. Moreover, the highly nonlinear electromechanical

coupling makes the problem even more complex and the fully multiphysics interaction must be considered in order to properly model the viscous and time-dependent electromechanical response; from this viewpoint, the physics-based micromechanical model described in the manuscript provides an effective and simple physics-based approach to solve this multiphysics issue.

The manuscript is organized as follows. First, we present the basic modeling relations for nonlinear electroelasticity, the main field-related quantities, and the related governing equations. Section “Statistics-based modeling of the mechanics of polymers” illustrates some concepts related to the statistics-based description of the mechanics of the chains network constituting the polymer and their extension to time-dependent networks produced by micromechanical interaction and relaxation. On the basis of a thermodynamic approach, it is proposed to quantify the network evolution on the basis of the applied deformation and on the kinetic parameters providing the rates of the internal remodeling phenomenon, accounting for the irreversible mechanisms occurring at the nanoscale level. In sections “Thermodynamics-based constitutive relations” and “FE implementation,” we discuss the electromechanical coupling and its numerical implementation, focusing on the simulation of materials with an evolving microstructure. Being the full coupling exploitable for instance in shape morphing technology, section “Numerical examples” presents some simple examples showing how the combination of an electric stimulus applied to a polymer with internally reorganizable network enables us to properly describe its time-dependent viscous response just by knowing few physics-based parameters. Finally, the last section outlines the main obtained results and critically discusses the proposed coupled approach for the mechanical modeling of electroactive visco-elastic polymers.

Electromechanical coupling in matter

Dielectric elastomer actuators (DEAs) are electromechanical materials capable of transforming electric energy to mechanical deformation (Carpi et al., 2008). The coupling between the mechanical and the electrical response is described by means of related forces. The contribution of these forces is typically proportional to the square of the electric field intensity, $|\mathbf{E}|$, weighted by the electric permittivity of the free space, ε_0 , times the elastomer's dielectric constant ε_r (Pelrine et al., 1998).

A typical arrangement of a DEA consists of a couple of compliant parallel plate electrodes with a dielectric material in-between; by applying an electric potential difference to the two plates, they become positively and negatively charged. As a main consequence, the two

above mentioned plates attract each other due to electrostatic forces and a mechanical stress is induced in the polymer. Moreover, if the material is polarizable, a further stress state arises because of the electric forces acting on the dipoles originating in the material. Furthermore, the deformation induced in the material itself influences and modifies the electric field, leading to a highly nonlinear coupled electromechanical problem.

The model for physically coupled electroactive behavior is suitable to be readily numerically implemented, such as through the finite element method (FEM). In this context, several models have been successfully developed and used to simulate various theoretical and practical situations (Ask et al., 2012a, 2012b; Thylander et al., 2012; Vu et al., 2007; Wissler and Mazza, 2007).

Main electric field-related quantities

In order to provide the basic background to the mathematical formulation of the electro-elastic coupling, a short introduction on the main quantities and field equations is provided hereafter. Let us consider a body in its undeformed configuration \mathbf{B}_0 ; each material point within the body is identified by the position vector \mathbf{X} in \mathbf{B}_0 while \mathbf{x} is the position vector in the current (deformed) configuration \mathbf{B}_t . The mapping of the motion of each material point from \mathbf{B}_0 to \mathbf{B}_t is given by the sufficiently regular vector function $\vartheta(\mathbf{X}, t)$, while the deformation gradient tensor is provided by $\mathbf{F} = \nabla_{\mathbf{X}}\vartheta(\mathbf{X}, t)$ (its determinant is indicated with $J = \det \mathbf{F} > 0$) and the referential mass density ρ_0 is related to the spatial mass density via $\rho_0 = \rho J$ (Ask et al., 2013).

Being the material immersed in an electric field, other quantities arise and assume a relevant role; in the deformed configuration, we can identify the electric field \mathbf{e} , the electric displacements \mathbf{d} , and the polarization vector \mathbf{p} , linked together by the well-known relation $\mathbf{d} = \varepsilon_0 \mathbf{e} + \mathbf{p}$, ε_0 being the permittivity of the vacuum. In vacuum, the polarization vanishes, that is, $\mathbf{p} = \mathbf{0}$, and the electric displacement results in $\mathbf{d} = \varepsilon_0 \mathbf{e}$ (Bustamante et al., 2008); as in the case in which the polarization \mathbf{p} is aligned with the electric field \mathbf{e} , $\mathbf{p} = \varepsilon_0 \chi \mathbf{e}$, the electric displacements can be expressed as $\mathbf{d} = \varepsilon_0 \varepsilon_r \mathbf{e}$, and if the relative permittivity (dielectric constant) $\varepsilon_r = 1 + \chi = \text{const.}$ (χ being the susceptibility), the dielectric elastomers are called linear dielectric. In the present paper, the material is assumed to be isotropic from both the electric as well as for the mechanical viewpoint. A dielectric material is able to develop dipoles under the action of an electric field; this propensity is represented by the polarizability, as expressed by the ratio of the induced dipole moment to the applied electric field (Dorfmann and Ogden, 2014). For an electrostatic problem in which no free charge is involved, high velocities and magnetic interactions are

neglected; the electric field \mathbf{e} is irrotational (i.e. it is such that $\nabla_{\mathbf{x}}^T \times \mathbf{e} = \mathbf{0}$), as it will be assumed henceforth, and the electric field can be obtained through a scalar (electric) potential Φ as follows

$$\mathbf{e} = -\nabla_{\mathbf{x}}\Phi \quad (1a)$$

while the corresponding material counterpart is given by

$$\mathbf{E} = -\nabla_{\mathbf{X}}\Phi = -\nabla_{\mathbf{X}}\Phi \frac{d\mathbf{x}}{d\mathbf{X}} = -\nabla_{\mathbf{X}}\Phi \mathbf{F} \quad (1b)$$

The relationship between the main electric field-related quantities measured in the material framework ($\mathbf{E}, \mathbf{D}, \mathbf{P}$) and their corresponding spatial counterparts ($\mathbf{e}, \mathbf{d}, \mathbf{p}$) is expressed as (Dorfmann and Ogden, 2014)

$$\begin{aligned} \mathbf{E} &= \mathbf{e}\mathbf{F}, \mathbf{D} = J \mathbf{d}\mathbf{F}^{-T}, \mathbf{P} = J \mathbf{p}\mathbf{F}^{-T} \quad \text{and} \\ \mathbf{D} &= J\varepsilon_0 \mathbf{E}(\mathbf{F}^{-1}\mathbf{F}^{-T}) + \mathbf{P} \end{aligned} \quad (2)$$

Moreover, we also have the following relevant balance relations (Gauss' law), $\nabla_{\mathbf{x}} \cdot \mathbf{d} = 0$, $\nabla_{\mathbf{X}} \cdot \mathbf{D} = 0$, stating that the electric displacements (in the deformed and in the reference configuration, \mathbf{d}, \mathbf{D} , respectively) constitute a divergence-free vector field.

The electric field and the corresponding electric displacements must also fulfill the following boundary conditions of the Neumann type on each surface of discontinuity present in the problem

$$[[\mathbf{D}]] \cdot \mathcal{N} = 0, \quad [[\mathbf{E}]] \times \mathcal{N} = \mathbf{0} \quad \text{on } \partial\mathbf{B}_0 \quad (3)$$

where $[[\mathbf{D}]]$, $[[\mathbf{E}]]$ indicate the jump of the electric displacement \mathbf{D} and of the electric field \mathbf{E} on $\partial\mathbf{B}_0$ and \mathcal{N} is the referential outward unit normal vector, respectively.

Balance of linear momentum in the presence of electro-mechanical coupling

In the presence of electromechanical interaction, the equilibrium equations cannot be written uniquely, and more than one single definition of the stress tensor is possible (Toupin, 1956). According to the so-called total stress tensor approach based on the two dipole model, the equations of balance of linear momentum, in the case of the existence of electromechanical interactions, can be expressed as follows

$$\nabla_{\mathbf{x}} \cdot \mathbf{T} + \rho_0 \mathbf{b} = \mathbf{0} \quad \text{in } \mathbf{B}_0 \quad (4)$$

where

$$\begin{aligned} \mathbf{T} &= \mathbf{P}_{Mech} + \mathbf{P}_{Mel} = \mathbf{P} + \varepsilon_0 \varepsilon_r J [\mathbf{e} \otimes \mathbf{e} - 1/2(\mathbf{e} \cdot \mathbf{e})\mathbf{I}] \mathbf{F}^{-T} = \\ &= \mathbf{P} + \varepsilon_0 \varepsilon_r J [\mathbf{F}^{-1}\mathbf{E} \otimes \mathbf{F}^{-1}\mathbf{E} - 1/2(\mathbf{F}^{-1}\mathbf{E} \cdot \mathbf{F}^{-1}\mathbf{E})\mathbf{I}] \mathbf{F}^{-T} \end{aligned} \quad (5)$$

where \mathbf{T} is the total first Piola stress tensor and \mathbf{P} denotes \mathbf{T} minus the stress contributions related to electrical body forces. The corresponding Neumann boundary conditions are

$$J^{-1}\mathbf{F}\mathbf{T}^T \cdot \frac{\mathbf{F}^{-T}\mathcal{N}}{\|\mathbf{F}^{-T}\mathcal{N}\|} = \mathbf{T}_{Mech} + \mathbf{T}_{Mel} \quad (6)$$

where \mathbf{T}_{Mech} and $\mathbf{T}_{Mel} = J^{-1}\mathbf{F}\mathbf{P}_{Mel}^T \cdot \mathbf{F}^{-T}\mathcal{N}/\|\mathbf{F}^{-T}\mathcal{N}\|$, \mathcal{N} are the vectors of the purely mechanical and of the electromechanical traction forces applied to the unconstrained portion of the boundary and the corresponding unit normal vector to $\partial\mathbf{B}_{0(f)}$, respectively.

In equation (4), \mathbf{b} represents the purely mechanical body force. It is worth mentioning that the presence of the electric-related body forces can also cause the Cauchy stress $\boldsymbol{\sigma} = J^{-1}\mathbf{P}\mathbf{F}^T$ to be unsymmetric.

The above-mentioned Maxwell Piola stress tensor \mathbf{P}_{Mel} corresponds to a further body force field \mathbf{b}_{e0} (forces per unit initial volume) arising due to the electromechanical interaction (Dorfmann and Ogden, 2005; Tiersten, 1971; Toupin, 1956)

$$\mathbf{b}_{e0} = \varepsilon_0 \varepsilon_r \cdot$$

$$\nabla_{\mathbf{x}} \cdot [\mathbf{E}\mathbf{F}^{-1} \otimes J^{-1}\mathbf{D}\mathbf{F}^T - 1/2\varepsilon_0(\mathbf{E}\mathbf{F}^{-1} \cdot \mathbf{E}\mathbf{F}^{-1})\mathbf{I}] \mathbf{F}^{-T} \quad (7)$$

In the case in which the permittivity of the material depends on the deformation, $\varepsilon_r = \varepsilon_r(\mathbf{F})$, the electromechanical stress contribution given by equation (5₂), expressed through the first Piola stress tensor contribution \mathbf{P}_{Mel} , must be rewritten to account for such a dependence, that is (Ask et al., 2015; Wissler and Mazza, 2007)

$$\begin{aligned} \mathbf{P}_{Mel} &= \varepsilon_0 \varepsilon_r J [\mathbf{F}^{-1}\mathbf{E} \otimes \mathbf{F}^{-1}\mathbf{E} - 1/2(\mathbf{F}^{-1}\mathbf{E} \cdot \mathbf{F}^{-1}\mathbf{E})\mathbf{I}] \mathbf{F}^{-T} \\ &\quad - \varepsilon_0 J(\mathbf{F}^{-1}\mathbf{E} \cdot \mathbf{F}^{-1}\mathbf{E})(\partial\varepsilon_r/\partial\mathbf{F}) \end{aligned} \quad (8)$$

Statistics-based modeling of the mechanics of polymers

Introduction

The mechanical response of an elastomer has been recognized to be driven by the deformation of its three-dimensional network made by cross-linked linear polymer chains; the geometrical description of such a complex 3D chain arrangement must be given in a probabilistic way, that is, not by giving its characteristics in a deterministic manner, while the random walk theory is the mathematical tool typically adopted to model the geometry of a single chain.

Polymer chain statistics represents a useful and common way to describe the mechanical behavior of elastomeric materials (such as natural rubbers, polymers, gels) with a microstructure made by a complex

entangled network of long linear chains reciprocally joined; it is worth noting that similar complex microstructures can also be observed in others materials, such as in biological matters and tissues, whose mechanical response can also be described based on the chain network approach (Kuhn, 1946; Kuhn and Grün, 1946).

We are here interested in modeling the viscoelastic behavior of the material through a physics-based micromechanical approach; the material is therefore assumed to lie in a general class of polymers made of a chain network whose topology can evolve over time. This evolution may be due to chain sliding, bond breaking and reforming, changes in chain entanglements. By considering the evolution of the chain arrangement as a dynamic process, the spatial elongation rate of the so-called chain's end-to-end distance vector \mathbf{r} over the small time interval dt is given by $\dot{\mathbf{r}} = \mathbf{L}\mathbf{r}$, with $\mathbf{L} = \partial \mathbf{v} / \partial \mathbf{x} = \dot{\mathbf{F}} \mathbf{F}^{-1}$, \mathbf{v} being the velocity vector field (Figure 1). In the remainder of this study, we refer to these events as chain attachment (to describe the formation of physical/chemical links between chains) and chain detachment (to describe the dissociation of such physical links).

From single chain to network

The mechanical state of a polymer chain is expressed in terms of its end-to-end distance \mathbf{r} . In the limit of long chains, the elastic energy stored in a chain of end-to-end distance \mathbf{r} is expressed by

$$\psi_c(\mathbf{r}) = \frac{3k_B T}{2nb^2} \mathbf{r}^2 \text{ or equivalently : } \psi_c(\mathbf{r}) = \frac{k_B T}{2} \tilde{r}^2 \quad (9)$$

where the normalized distance is given by $\tilde{r} = |\mathbf{r}|/\ell = r/\ell$, $\ell = b\sqrt{n/3}$ is the projected mean end-to-end distance $b\sqrt{n}$ of each individual chain, n is the number of Kuhn segments of a chain, and b is Kuhn's length. To describe the mechanical behavior of the network, we assume that a material point is associated with an initially isotropic population of polymer chains whose configurations at the generic time t are described by a distribution function

$$\varphi(\mathbf{r}, t) = c(t) \cdot P(\mathbf{r}, t) \quad (10)$$

that describes, in an average sense, the proportion of chain with an end-to-end vector comprised between \mathbf{r} and $\mathbf{r} + d\mathbf{r}$. In equation (10), c characterizes the concentration of mechanically active (or attached) polymer chains, while $P(\mathbf{r}, t)$ is the normalized distribution, or probability function.

We see here that the distribution function is allowed to vary with time due to the chain detachment and attachment events. For an isotropic polymer with long chains, moreover, the chain distribution in its stress-free

state does not depend on direction and the probability function becomes a Gaussian (Kuhn and Grün, 1946; Vernerey et al., 2017)

$$P_0(\mathbf{r}) = \left(\frac{3}{2\pi nb^2} \right)^{3/2} \cdot \exp \left(-\frac{3|\mathbf{r}|^2}{2nb^2} \right) \quad (11)$$

The distribution φ_0 of chains in their stress-free state at the time instant t_0 can therefore be related to the function P_0 by

$$\varphi_0(\mathbf{r}, t_0) = c(t_0) \cdot P_0(\mathbf{r}) \quad (12)$$

We have shown in a previous study (Vernerey et al., 2017) that the link between a single chain and the network can be established via the integration $\langle \bullet \rangle$ that spans all the chains' end-to-end distances and directions in the form

$$\langle \bullet \rangle = \int_0^{2\pi} \int_0^\pi \left(\int_0^{+\infty} \bullet r^2 dr \right) \sin \theta d\theta d\omega \quad (13)$$

where the angles θ and ω are the polar angles defining the direction of a single chain. With this operation, it can be shown that the integral of the probability function $\langle P(\mathbf{r}, t) \rangle = 1$ and, therefore, the chain concentration can be directly found by

$$c(t) = \langle \varphi(\mathbf{r}, t) \rangle \quad (14)$$

If the material is isotropic, the function $P(\mathbf{r}, t)$ (and consequently $\varphi(\mathbf{r}, t)$) can be expressed only in terms of $r = |\mathbf{r}|$; this assumption is assumed hereafter in the paper.

Distribution tensor and network mechanics

A good indication of the amount of stretch experienced by chains in the network is given by the so-called distribution tensor $\boldsymbol{\mu}$ written in the form (Vernerey et al., 2017)

$$\boldsymbol{\mu}(t) = \langle P(r, t) \tilde{\mathbf{r}} \otimes \tilde{\mathbf{r}} \rangle \quad (15)$$

where $\tilde{\mathbf{r}} = \mathbf{r}/(b\sqrt{n/3})$, $b\sqrt{n}$ being the projected mean end-to-end distance of individual chains.

With this definition, it can be shown that in the stress-free state, that is, when the probability function is described by equation (11), the distribution tensor degenerates to $\boldsymbol{\mu}(t_0) = \boldsymbol{\mu}_0 = \mathbf{I}$; here \mathbf{I} is the second-order identity tensor. For sake of simplifying the notation, in the following we omit to specify the time dependence, assuming that a generic deformed configuration of the material takes place at a time $t > t_0$. Based on the distribution tensor, it is possible to evaluate the strain energy stored in the network based on equation (9) as

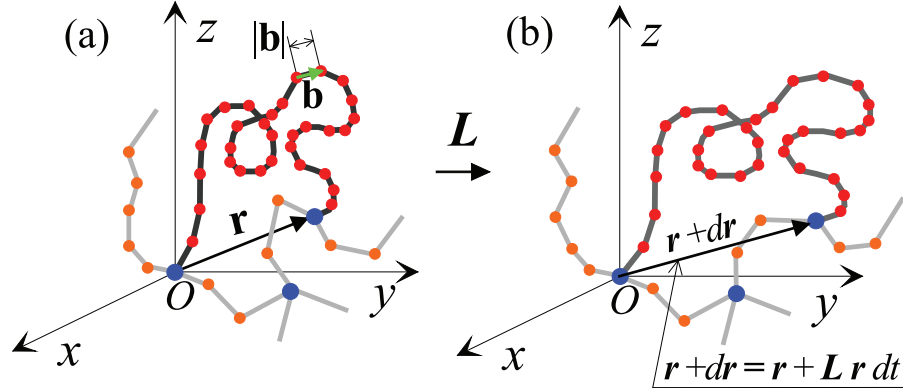


Figure 1. Scheme of the deformation occurring on a single polymeric chain due to mechanical stretch represented by the velocity gradient \mathbf{L} : (a) undeformed state and (b) deformed state after the time dt .

$$\psi(\mathbf{r}) = \frac{ck_B T}{2} \text{tr}(\boldsymbol{\mu} - \mathbf{I}) \quad (16)$$

and the corresponding Cauchy and Piola stress tensors, for an incompressible polymer, are

$$\boldsymbol{\sigma} = ck_B T (\boldsymbol{\mu} - \mathbf{I}) + p\mathbf{I} \quad (17a)$$

$$\mathbf{P} = J[ck_B T (\boldsymbol{\mu} - \mathbf{I})\mathbf{F}^{-T} + p\mathbf{F}^{-T}] \quad (17b)$$

where p is the pressure-like Lagrange multiplier enforcing the incompressibility condition $\dot{J} = J \text{tr}(\mathbf{S}) = 0$, and $\mathbf{S} = (\dot{\mathbf{F}}\mathbf{F}^{-1})^s = 1/2(\mathbf{L} + \mathbf{L}^T)$ is the symmetric part of the spatial velocity gradient tensor \mathbf{L} .

Since we are considering a material in which its internal microstructure evolves in time, a unique reference state of the material does not exist, and the above equations have to be more conveniently considered from an incremental viewpoint, rather than for a finite deformation, as shown below.

Internal material evolution through bond dynamics

For dynamic polymers experiencing changes in their network topology due, for instance, to chain sliding, bond breaking and reforming, ... the chain distribution evolves. This means that the density of mechanically active chains c may also change with time. In this work, it is assumed that a single chain's dynamics are represented by a rate of detachment k_D and a rate of attachment k_A . When an active chain detaches, it becomes inactive and the overall concentration c of active chains decreases. When an inactive chain reattaches, however, it raises the concentration c . Using a first-order kinetic law, we have shown in Vernerey et al. (2017) that the material derivative of the concentration c can be written as

$$\dot{c} = k_A (c^t - c) - k_D c \quad (18)$$

where c^t is the maximum number of potentially mechanically active chains in the network.

In the particular case in which $k_A = k_D$, the material reconfigures itself in time, and the polymer is characterized by a so-called bond exchange reaction: in this case, an attachment event, occurring in the stress-free configuration, is immediately followed by a detachment one, arising from the deformed configuration. This implies that the number of attached chains remains constant in time and the material always maintains a positive stiffness.

Furthermore, using the fact that active chains detached in their stretched state (under force) but reattached in a stress-free state (force-free), an evolution equation could be derived for the distribution tensor (Vernerey et al., 2017)

$$\dot{\boldsymbol{\mu}} = \mathbf{S}\boldsymbol{\mu} + \boldsymbol{\mu}\mathbf{S} - \left(\frac{\dot{c}}{c} + k_D\right)\boldsymbol{\mu} = (\dot{\mathbf{F}}\mathbf{F}^{-1})^s\boldsymbol{\mu} + \boldsymbol{\mu}(\dot{\mathbf{F}}\mathbf{F}^{-1})^s - \left(\frac{\dot{c}}{c} + k_D\right)\boldsymbol{\mu} \quad (19)$$

where $\dot{\boldsymbol{\mu}}$ has been written through the symmetric part \mathbf{S} of the spatial velocity gradient \mathbf{L} .

In other words, changes in the overall network configuration are affected by the strain rate (represented by the symmetric part of the velocity deformation gradient \mathbf{S}) and by the bond dynamic through the last terms in equation (19). We note that the bond dynamic leads to a general stress relaxation that can be measured by the mechanical energy dissipation (Vernerey et al., 2017)

$$\mathcal{D} = k_D \frac{ck_B T}{2} \text{tr}(\boldsymbol{\mu} - \mathbf{I}) = k_D \psi(\mathbf{r}) \quad (20)$$

The above presented approach of the time-dependent behavior of the polymer can be generalized by assuming the existence of multiple networks, that is, different non-interacting networks characterized by different bond dynamic parameters k_D , k_A (Vernerey et al.,

2017). In particular, in the present study, the existence of a static network (i.e. with $k_D = k_A = 0$, whose volume fraction in the polymer is indicated with f_c) is assumed to coexist with a dynamic one with volume fraction $f_d = 1 - f_c$.

Thermodynamics-based constitutive relations

In the present section, the main constitutive relationships for an electroactive viscoelastic polymer are derived starting from the general thermodynamical relations related to the principle of energy balance and to the principle of non-decreasing entropy in a closed system. We recall here that the dissipation phenomenon representing the viscosity behavior in the material is assumed to be represented by the internal network remodeling feature.

Basic thermodynamical relationships and stress state

According to the second law of thermodynamics, for every process taking place in the body that occupies volume Ω , the following Clausius–Duhem inequality must be satisfied

$$\dot{\gamma}(t) = \dot{S}(t) - \bar{Q}(t) \geq 0, \text{ with } S(t) = \int_{B_t} \eta(\mathbf{x}, t) d\Omega \quad (21)$$

It states that the entropy production rate $\dot{\gamma}(t)$ in Ω is always non-negative; in equation (21), $\eta(\mathbf{x}, t)$ is the entropy per unit volume and $\bar{Q}(t) = - \int_{\partial B_t} (\dot{\mathbf{q}}/T) \cdot \mathbf{n} ds + \int_{B_t} \dot{Q}/T d\Omega$ is the rate of entropy input, with $\dot{\mathbf{q}}$ and \dot{Q} being the rates of boundary heat flux and volume heat sources, respectively. For sake of simplicity, in the following, we assume that no flux or production of heat exists, that is, $\dot{\mathbf{q}} = \mathbf{0}$ and $\dot{Q} = 0$; furthermore, we adopt the polarization to be parallel to the electric field and consequently, the electric displacements are written as $\mathbf{d} = \varepsilon_0 \varepsilon_r \mathbf{e}$.

Let us now introduce the Helmholtz free energy per unit reference volume

$$A = \mathcal{E} - T \cdot \eta(\mathbf{x}, t) \quad (22)$$

in which \mathcal{E} represents the internal energy per unit reference volume of the body. A so-called augmented free energy is herein introduced according to Dorfmann and Ogden (2005)

$$\begin{aligned} \Psi(\mathbf{F}, \mathbf{E}) &= \psi - 1/2 \varepsilon_0 J (\mathbf{E} \cdot \mathbf{C}^{-1} \mathbf{E}) = \\ &= [\mathcal{E}_{Mech}(\boldsymbol{\mu}) + \mathcal{E}_{MEI}(\mathbf{F}, \mathbf{E}) + \mathcal{E}_{El}(\mathbf{E}) - T \cdot \eta(\mathbf{x}, t)] \\ &- 1/2 \varepsilon_0 J (\mathbf{E} \cdot \mathbf{C}^{-1} \mathbf{E}) \end{aligned} \quad (23)$$

where $\dot{\mathcal{E}}_{Mech}(\boldsymbol{\mu}) = \boldsymbol{\sigma} : \mathbf{L} = \mathbf{P} : \dot{\mathbf{F}}$ is the rate of the purely mechanical contribution to the energy, $\mathcal{E}_{MEI}(\mathbf{F}, \mathbf{E})$ the electro-elastic coupled contribution, $\mathcal{E}_{El}(\mathbf{E})$ the purely electric contribution, and the last term represents the free space effect (being $\mathbf{C} = \mathbf{F}^T \mathbf{F}$ the right Cauchy–Green deformation tensor). By assuming that the process is isothermal (i.e. $\dot{T} = 0$), the time derivative of the augmented free energy is

$$\dot{\Psi} = \underbrace{\{\boldsymbol{\sigma} + \varepsilon_0 \varepsilon_r [\mathbf{e} \otimes \mathbf{e} - 1/2(\mathbf{e} \cdot \mathbf{e})\mathbf{I}]\}}_{\boldsymbol{\tau}} : \dot{\mathbf{F}} \mathbf{F}^{-1} + \dot{\mathcal{E}}_{El}(\mathbf{E}) - \mathcal{D} \quad (24)$$

where

$$\mathcal{D} = \boldsymbol{\tau} : \dot{\mathbf{F}} \mathbf{F}^{-1} - \dot{\Psi} = k_D \frac{ck_B T}{2} \text{tr}(\boldsymbol{\mu} - \mathbf{I}) = k_D \psi_{Mech}(\mathbf{r}) \geq 0 \quad (25)$$

is the rate of energy dissipation that corresponds to the Clausius–Duhem inequality (21), and the rate of mechanical energy accounting for both the deformation rate and the internal remodeling feature of the material is (Vernerey et al., 2017)

$$\dot{\mathcal{E}}_{Mech}(\dot{\mathbf{F}}) = \boldsymbol{\sigma} : \mathbf{L} = \frac{ck_B T}{2} (\boldsymbol{\mu} - \boldsymbol{\mu}_0) : \mathbf{L} + p \text{tr}(\mathbf{L}) \quad (26)$$

The above defined stress tensor $\boldsymbol{\tau} = \boldsymbol{\sigma} + \boldsymbol{\sigma}_{MEI}$ has the corresponding counterpart two point tensor \mathbf{T} that can be expressed as

$$\begin{aligned} \mathbf{T} &= \mathbf{P}_{Mech} + \mathbf{P}_{MEI} = J \boldsymbol{\tau} \mathbf{F}^{-T} = \\ &= J \left\{ \underbrace{[ck_B T(\boldsymbol{\mu} - \boldsymbol{\mu}_0) + p\mathbf{I}]}_{\boldsymbol{\sigma}} \right. \\ &\quad \left. + \underbrace{\varepsilon_0 \varepsilon_r [\mathbf{F}^{-1} \mathbf{E} \otimes \mathbf{F}^{-1} \mathbf{E} - 1/2(\mathbf{F}^{-1} \mathbf{E} \cdot \mathbf{F}^{-1} \mathbf{E})\mathbf{I}]}_{\boldsymbol{\sigma}_{MEI}} \right\} \mathbf{F}^{-T} \end{aligned} \quad (27)$$

In equation (27), $\boldsymbol{\sigma} = ck_B T(\boldsymbol{\mu} - \boldsymbol{\mu}_0) + p\mathbf{I}$ is the purely mechanical stress and $\boldsymbol{\sigma}_{MEI}$ is the electromechanical coupling stress (Dorfmann and Ogden, 2014). On the other hand, the referential electric displacement vector can be obtained through the following derivation

$$\mathbf{D} = - \frac{\partial \Psi(\mathbf{F}, \mathbf{E})}{\partial \mathbf{E}} : = \varepsilon_0 \varepsilon_r J \mathbf{E} \mathbf{C}^{-1} \quad (28)$$

where the polarization \mathbf{P} has been assumed to be in the same direction of the electric field \mathbf{E} . Note that the particularization of the referential electric displacements in (28) is assumed based on which of the remaining electrical energy contributions could be specified.

FE implementation

The above presented physics-based micromechanical model has been implemented in a homemade finite element program within a Lagrangian framework formulation. The degrees of freedom of each node are represented by both the displacements and the electric potential, while the Dirichlet boundary conditions for the solution of the electrostatic problem are applied to the solid, and the corresponding Maxwell stress are accounted for in the solution of the mechanical problem through an iterative procedure. The coupled electrical and the mechanical problems are solved in sequence in the iteration loops required for the solution of the nonlinear electromechanical problem. The electric field is determined by accounting for the deformed domain of the problem, and the corresponding Maxwell stresses are included in the expression of the unbalanced nodal force vector.

The coupled governing equations for the problem under study can be obtained starting from the weak form expressions of the mechanical and of the electric balance (here written in the hypothesis of absence of free body or surface charges)

$$\delta W_{Mech} = \int_{B_0} \nabla_X \delta \alpha : \mathbf{T} dV - \int_{B_0} \rho_0 \delta \alpha \cdot \mathbf{b} dV - \int_{\partial B_0} \delta \alpha \cdot \mathbf{T} d\Gamma = 0 \quad (29a)$$

$$\delta W_{El} = - \int_{B_0} \nabla_X \delta \Phi \cdot \mathbf{D} dV - \int_{\partial B_0} \delta \Phi \cdot D_{\mathcal{N}} d\Gamma = 0 \quad (29b)$$

where $\delta \alpha$ and $\delta \Phi$ are the virtual displacement field and the virtual electric potential field, respectively, and $D_{\mathcal{N}} = -\mathbf{D} \cdot \mathcal{N}$ is the electric charge on the boundary with outward normal \mathcal{N} . By introducing the finite element discretization of the reference domain, the governing equations can be finally obtained; for a single finite element, the above-mentioned equations written in the reference configuration at a given time t corresponding to a particular load step are

$$\begin{cases} \delta \mathbf{u}^T \cdot \int_{B_{0e}} \mathbf{B}^T \mathbf{T} dV = \delta \mathbf{u}^T \cdot \int_{B_{0e}} \rho_0 \mathbf{N}^T \mathbf{b} dV + \delta \mathbf{u}^T \cdot \int_{\partial B_{0e}} \mathbf{N}^T \mathbf{T} d\Gamma \\ \delta \Phi^T \cdot \int_{B_{0e}} \tilde{\mathbf{B}}^T \mathbf{D} dV = \delta \Phi^T \cdot \int_{B_{0e}} \tilde{\mathbf{B}}^T (\varepsilon_0 \varepsilon_r) \tilde{\mathbf{B}} \mathbf{J} \mathbf{C}^{-1} dV \cdot \Phi = - \delta \Phi^T \cdot \int_{\partial B_{0e}} \tilde{\mathbf{N}}^T D_{\mathcal{N}} d\Gamma \end{cases} \quad (30a)$$

$$\quad (30b)$$

with the corresponding mechanical Dirichlet and Neumann boundary conditions and the Dirichlet

boundary condition $\Phi_n(t) = \bar{\Phi}_n(t)$ on $\partial B_{0e}(\Phi)$ for the electric problem, respectively; B_{0e} , ∂B_{0e} are the volume of the initial domain and traction boundary of the finite element e in turn, while the virtual displacement and the virtual electric potential fields have been expressed through the corresponding nodal values, $\delta \alpha = \mathbf{N} \delta \mathbf{u} = \sum_{i=1}^{n_{en}} N_i \delta \mathbf{u}_i$ and $\delta \Phi = \tilde{\mathbf{N}} \delta \Phi = \sum_{i=1}^{n_{en}} \tilde{N}_i \delta \Phi_i$. In equations (30a) and (30b), $\mathbf{B} = \nabla_X \mathbf{N}$ and $\tilde{\mathbf{B}} = \nabla_X \tilde{\mathbf{N}}$ are the compatibility matrices related to the mechanical and electrical fields, respectively, and \mathbf{N} , $\tilde{\mathbf{N}}$ are the element shape functions for the interpolation of the mechanical and electrical displacements, respectively. The equilibrium equations (30a) and (30b) are written under the assumption of quasi-static conditions for the external mechanical actions as well as of the potential $\bar{\Phi}_n(t)$ in order to rule out any possible inertial effect.

The numerical solution of the coupled nonlinear problem requires to calculate the so-called unbalanced nodal force vector \mathbf{R}_e and the unbalanced nodal electric vector \mathbf{V}_e which are made to vanish over the iterations performed across the increments of the external actions (electrical and/or mechanical); referred to a single finite element, from equations (30a) and (30b), they can be expressed as

$$\mathbf{R}_e = \int_{B_{0e}} (\mathbf{B}^T \mathbf{T} - \rho_0 \mathbf{N} \mathbf{b}) dV - \int_{\partial B_{0e}} \mathbf{N}^T \mathbf{T} d\Gamma \neq \mathbf{0} \quad (31a)$$

$$\mathbf{V}_e = \int_{B_{0e}} \tilde{\mathbf{B}}^T (\varepsilon_0 \varepsilon_r \mathbf{J} \mathbf{E} \mathbf{C}^{-1}) dV + \int_{\partial B_{0e}} \tilde{\mathbf{N}}^T D_{\mathcal{N}} d\Gamma \neq \mathbf{0} \quad (31b)$$

By writing the spatial approximation of the field quantities and of their material gradient involved in the above balance equations, in terms of the corresponding finite element's nodal values

$$\begin{aligned} \mathbf{u}(\mathbf{X}) \approx \mathbf{u}^h(\mathbf{X}) &= \sum_{i=1}^{n_{en}} N_i(\mathbf{X}) \mathbf{u}_i, & \Phi(\mathbf{X}) \approx \Phi^h(\mathbf{X}) \\ &= \sum_{i=1}^{n_{en}} \tilde{N}_i(\mathbf{X}) \Phi_i \end{aligned} \quad (32a)$$

$$\quad (30a)$$

$$\quad (30b)$$

$$\begin{aligned}\nabla_{\mathbf{X}}\mathbf{u}(\mathbf{X}) &\approx \nabla_{\mathbf{X}}\mathbf{u}^h(\mathbf{X}) = \sum_{i=1}^{n_{en}} \nabla_{\mathbf{X}} N_i(\mathbf{X}) \mathbf{u}_i = \sum_{i=1}^{n_{en}} \mathbf{B}_i(\mathbf{X}) \mathbf{u}_i \\ \nabla_{\mathbf{X}}\Phi(\mathbf{X}) &\approx \nabla_{\mathbf{X}}\Phi^h(\mathbf{X}) = \sum_{i=1}^{n_{en}} \nabla_{\mathbf{X}} \tilde{N}_i(\mathbf{X}) \Phi_i = \sum_{i=1}^{n_{en}} \tilde{\mathbf{B}}_i(\mathbf{X}) \Phi_i\end{aligned}\quad (32b)$$

and by linearizing the balance equations (30a) and (30b) expressed in incremental form, the tangent stiffness matrix of the finite element e can be identified; it assumes the following structure

$$\mathbf{k}'|_{\mathbf{B}_{0e}} = \begin{bmatrix} \mathbf{k}'_{Mech} & \mathbf{k}'_{MEI} \\ \mathbf{k}'_{EIM} & \mathbf{k}'_{El} \end{bmatrix}_{\mathbf{B}_{0e}} \quad (33)$$

in which the submatrices in $\mathbf{k}'|_{\mathbf{B}_{0e}}$ are given by (Haldar et al., 2016)

$$\begin{aligned}\mathbf{k}'_{Mech}|_{\mathbf{B}_{0e}} &= \sum_{i=1}^{n_{en}} \sum_{j=1}^{n_{en}} \int_{\mathbf{B}_{0e}} \nabla_{\mathbf{X}} N_i \mathbf{C}'_{Mech} \nabla_{\mathbf{X}} N_j dV \\ \mathbf{k}'_{MEI}|_{\mathbf{B}_{0e}} &= \sum_{i=1}^{n_{en}} \sum_{j=1}^{n_{en}} \int_{\mathbf{B}_{0e}} \nabla_{\mathbf{X}} N_i \mathbf{C}'_{MEI} \nabla_{\mathbf{X}} \tilde{N}_j dV \\ \mathbf{k}'_{EIM}|_{\mathbf{B}_{0e}} &= \sum_{i=1}^{n_{en}} \sum_{j=1}^{n_{en}} \int_{\mathbf{B}_{0e}} \nabla_{\mathbf{X}} \tilde{N}_i \mathbf{C}'_{EIM} \nabla_{\mathbf{X}} N_j dV \\ \mathbf{k}'_{El}|_{\mathbf{B}_{0e}} &= \sum_{i=1}^{n_{en}} \sum_{j=1}^{n_{en}} \int_{\mathbf{B}_{0e}} \nabla_{\mathbf{X}} \tilde{N}_i \mathbf{C}'_{El} \nabla_{\mathbf{X}} \tilde{N}_j dV\end{aligned}\quad (34)$$

where N_m (\tilde{N}_m) is the element's shape functions referred to node m , while n_{en} is the number of nodes defining the finite element e . The tangent tensors \mathbf{C}'_{\dots} in equation (34) can be evaluated as (Haldar et al., 2016)

$$\begin{aligned}\mathbf{C}'_{Mech}(\mathbf{X}) &= \frac{\partial \mathbf{T}(\mathbf{X})}{\partial \mathbf{F}} = \frac{\partial (\mathbf{P}_{Mech}(\mathbf{X}) + \mathbf{P}_{MEI}(\mathbf{X}))}{\partial \mathbf{F}} \\ &= \frac{\partial^2 \mathcal{E}_{Mech}(\mathbf{X}, \mathbf{F})}{\partial \mathbf{F} \otimes \partial \mathbf{F}} \\ \mathbf{C}'_{MEI}(\mathbf{X}) &= \frac{\partial \mathbf{T}(\mathbf{X})}{\partial \mathbf{E}} = - \frac{\partial^2 \mathcal{E}_{MEI}(\mathbf{X}, \mathbf{F}, \mathbf{E})}{\partial \mathbf{E} \otimes \partial \mathbf{F}}; \\ \mathbf{C}'(\mathbf{X})_{EIM} &= \frac{\partial \mathbf{D}}{\partial \mathbf{F}} = - \frac{\partial^2 \mathcal{E}_{MEI}(\mathbf{X}, \mathbf{F}, \mathbf{E})}{\partial \mathbf{F} \otimes \partial \mathbf{E}} \\ \mathbf{C}'_{El}(\mathbf{X}) &= - \frac{\partial^2 \mathcal{E}_{El}(\mathbf{X}, \mathbf{E})}{\partial \mathbf{E} \otimes \partial \mathbf{E}} - 1/2 \varepsilon_0 \varepsilon_r J \mathbf{C}^{-1} = J \varepsilon_0 \varepsilon_r \mathbf{C}^{-1}\end{aligned}\quad (35)$$

where the dependence on the position \mathbf{X} has been introduced to underline the eventual dependence of a material property to the point location for a non-homogeneous material.

The above presented formulation provides the coupled discretized electric and mechanical equations involved in the problem under consideration; however, as has been recalled at the beginning of this section, the governing equations of the electric and of the

mechanical problem can be more conveniently solved in sequence in a stepwise staggered calculation.

Numerical examples

The presented formulation, dealing with the electromechanical coupled problem in which the time-dependent mechanical viscoelastic behavior is represented through the internal remodeling evolution of the material, has been implemented in a two-dimensional finite element homemade code.

A circular plate actuator problem is first solved by considering both the elastic and the viscoelastic behavior of the material, the latter modeled by assuming different relaxation parameters; the parametric analyses performed provide a useful insight into the macroscopic behavior obtained from the micromechanical evolution of the material. The second example considers a simple elastomeric block under an elastic potential history applied to its boundary; both slow and fast kinetic microscale evolution of the material are assumed and the electric potential as well as the stress field within the material is determined and analyzed. The last case considered is that of a beam-like actuator whose response is discussed and compared with the available literature results. In the numerical analyses, the Poisson's coefficient - whose conventional physical meaning is established in the linear elastic small deformation limit - has been assumed slightly lower than the value required by the incompressibility condition, because of the decreasing trend shown by such a coefficient with the strain increasing (Beatty and Stalnaker, 1986) and in order to avoid numerical instability issues of the model. In particular, Poisson's coefficient has been used in writing the tangent tensors \mathbf{C}'_{Mech} of the material.

Circular plate actuator

The first example considered is a simply supported elastomeric circular plate, with radius R and thickness w , operating as an electroactive actuator (Figure 2(a)). A couple of compliant circular electrodes with radius r_0 are applied to the plate as shown in the figure, that is, one on the top surface and the other in the plate's middle plane. The circular plate is characterized by the following geometrical dimensions $R = 10$ mm, $w = 1$ mm, and $r_0 = 3$ mm, while the material has the following mechanical properties: initial elastic modulus $E_0 = 0.5$ MPa, Poisson's ratio $\nu = 0.45$, relative electric permittivity equal to $\varepsilon_r = 10$. Large displacements are accounted for throughout the numerical analyses.

Both linear elastic and nonlinear elastic (hyperelastic, following the neo-Hookean model obtained by setting $k_A = k_D = 0.0$ (Vernerey et al., 2017)) models are used, while the viscoelastic behavior is modeled by adopting the time evolution of the material's internal cross-links as explained in section "Internal material

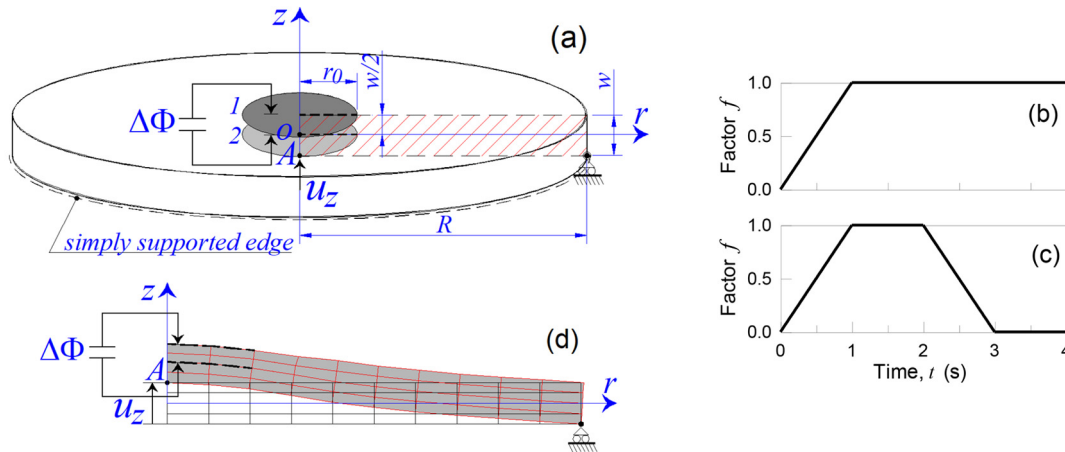


Figure 2. Simply supported circular plate with an electric potential applied to the two compliant electrodes (a). Scheme of the electric potential versus time applied to the electrodes (b, c). In (b), the potential reaches the steady state after 1 s, while in (c) the potential completes a full cycle in 3 s. Schematic sketch of the deformed shape of the plates after the application of the electric potential (d).

evolution through bond dynamics.” A fraction $f_d = 1 - f_c = 0.8$ of the total polymer’s cross-links per unit volume is assumed to be able to evolve in time, while the rearrangement kinetics are governed by the following bonds exchange rates: (1) $k_A = k_D = 1.0$ (slow kinetic remodeling rate), (2) $k_A = k_D = 5.0$ (medium kinetic remodeling rate), and (3) $k_A = k_D = 10.0$ (fast kinetic remodeling rate). The numerical integration of the electromechanical governing equations is performed by adopting a time step size equal to $\Delta t = 2 \times 10^{-2}$ s.

The time-variation of the electric potential intensity is assumed to be expressed by a relation of the form $\Delta\Phi(t) = \Delta\Phi_0 \cdot f(t)$, where the reference potential $\Delta\Phi_0 = 20$ kV and $f(t)$ is a time-dependent function illustrated in Figure 2(b) and (c) for the case in which a steady state or a cycle of the applied potential is assumed, respectively. The response of the plate, discretized through axisymmetric four-noded finite elements, is monitored by measuring the vertical displacement u_z at point A placed on the center of its bottom surface (Figure 2(a) and (d)).

In Figure 3, the dimensionless upward vertical displacement at point A versus time is represented for the two electric potential time histories displayed in Figure 2(b) and (c); different material behaviors are assumed (linear elastic, hyperelastic, and viscoelastic with different kinetic rates $k_A = k_D$). It can be noted that in the viscoelastic case, the displacement reaches higher values, and that in the case of fastest cross-links kinetic (to be interpreted as an internal material’s rearrangement for simulating the viscous behavior), the material reaches the steady state in a shorter time with respect to the slower kinetic case (dashed red lines in Figure 3(a) and (b)). It is worth noting that if the kinetics of the polymer chains rearrangement are much faster than those of

the applied load, the material behaves like a viscous fluid, while for intermediate values the standard viscoelastic behavior is recovered (Vernerey et al., 2017).

The asymptote approached by applying the electric potential history given in Figure 2(b) is due to the presence of a fraction ($f_c = 1 - f_d = 0.2$) of non-evolving (i.e. constant) cross-links that are permanently available in the load bearing polymer network volume; on the other hand, the evolving volume fraction of the polymer progressively relaxes its stress state and therefore does not contribute to the stiffness of the material.

Elastomeric block under a boundary electric potential history

The second example deals with the mechanical response of a simple plane stress elastomeric block of material (Figure 4(a) and (b)) subjected to a prescribed boundary electric potential time history (Figure 4(c)); since the block is subjected to a self-equilibrated surface pressure distribution generated by the applied electric potential, no mechanical restraints are required in the numerical simulation. A plane stress condition is assumed, while the geometrical characteristics of the element are such that $a = 100$ mm, $w = 30$ mm, while the upper electrode has a size $a' = 0.4a$ and the bottom one extends over the entire edge of the block (see dashed lines in Figure 4(a)). The material is assumed to have internal remodeling features with $f_d = 1 - f_c = 0.9$, while the initial elastic modulus is $E_0 = 0.1$ MPa, Poisson’s ratio $\nu = 0.45$, and the relative electric permittivity has been assumed equal to $\epsilon_r = 35$. The adopted mechanical parameters are typical of soft elastomers, such as in weakly reticulated silicone rubbers; such a low elastic modulus value allows

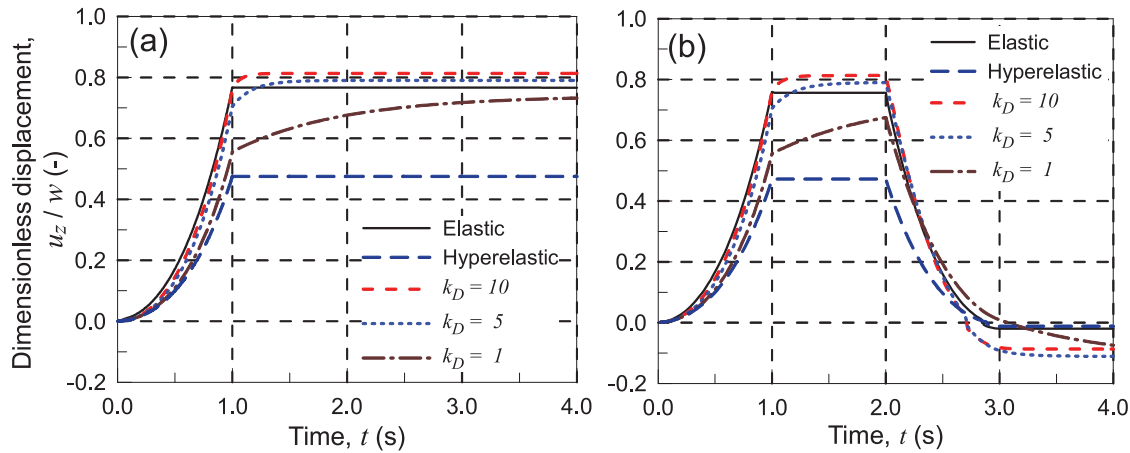


Figure 3. Dimensionless vertical displacement at point A for the elastomeric plate behaving as linear elastic, hyperelastic or viscoelastic material under the electric potential history illustrated in Figure 2(b) (a) and under the electric potential cycle illustrated in Figure 2(c) (b). Different values of the kinetic rates $k_A = k_D$ are adopted to model various degrees of viscoelasticity of the material.

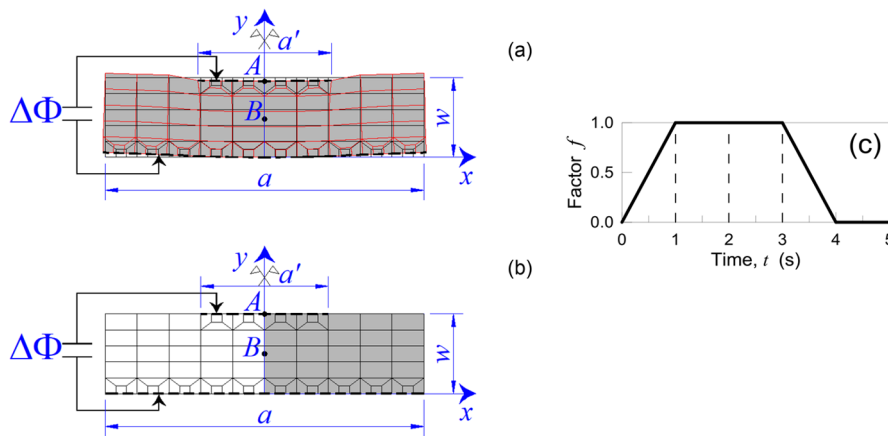


Figure 4. Elastomeric body with boundary prescribed electric potential; undeformed (a) and generic deformed configuration (b). The electric potential is made to vary in time as shown in (c).

for the development of large deformations under the effect of an applied electric potential. Large displacements are accounted for throughout the numerical calculations.

The dynamic fraction of the polymeric cross-links is assumed to comply with the rearrangement kinetics in time according to the following exchange rates: case 1— $k_A = k_D = 1.0$ (slow kinetic remodeling rate) and case 2— $k_A = k_D = 5.0$ (medium kinetic remodeling rate). The numerical integration of the electromechanical governing equations is performed by adopting a time step size equal to $\Delta t = 2 \times 10^{-2}$ s.

The variation of the intensity of the electric potential in time is assumed to be expressed by a relation of the form $\Delta\Phi(t) = \Delta\Phi_0 \cdot f(t)$, where the reference electric field $E_0 = \Delta\Phi_0/w = 2$ MV/m and $f(t)$ is a time-dependent function illustrated in Figure 4(b). Due to

the symmetry of the problem, only one half of the body has been discretized.

The response of the body, discretized through plane stress finite elements, is represented through the vertical displacement u_y at point A placed in the center of the upper electrode and by the mechanical stress arising at point B in the middle of the element (Figure 5(a) and (b)). In the case of the faster remodeling kinetic (case 2), it can be seen that the displacement is greater than in the case of slow internal rearrangement and, correspondingly, the stress remains always lower because of the stronger capability of the material to reset its internal microstructure in time.

It is worth noting that during the phase of constant applied potential value ($1 \leq t \leq 3$), the stress decreases and in the case of fast kinetics, the material has enough time to reach a steady state due to the presence of the

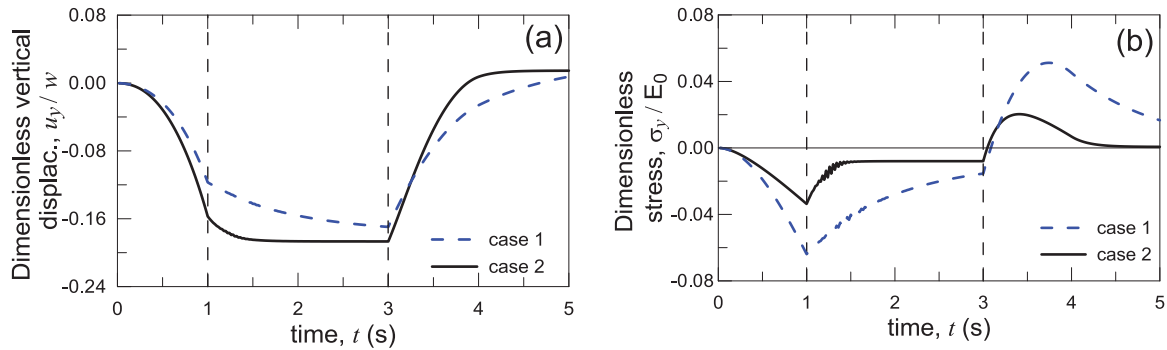


Figure 5. Vertical displacement at point A (see Figure 4(a)) for the two kinetic cases considered (a). Mechanical dimensionless stress history at B (b).

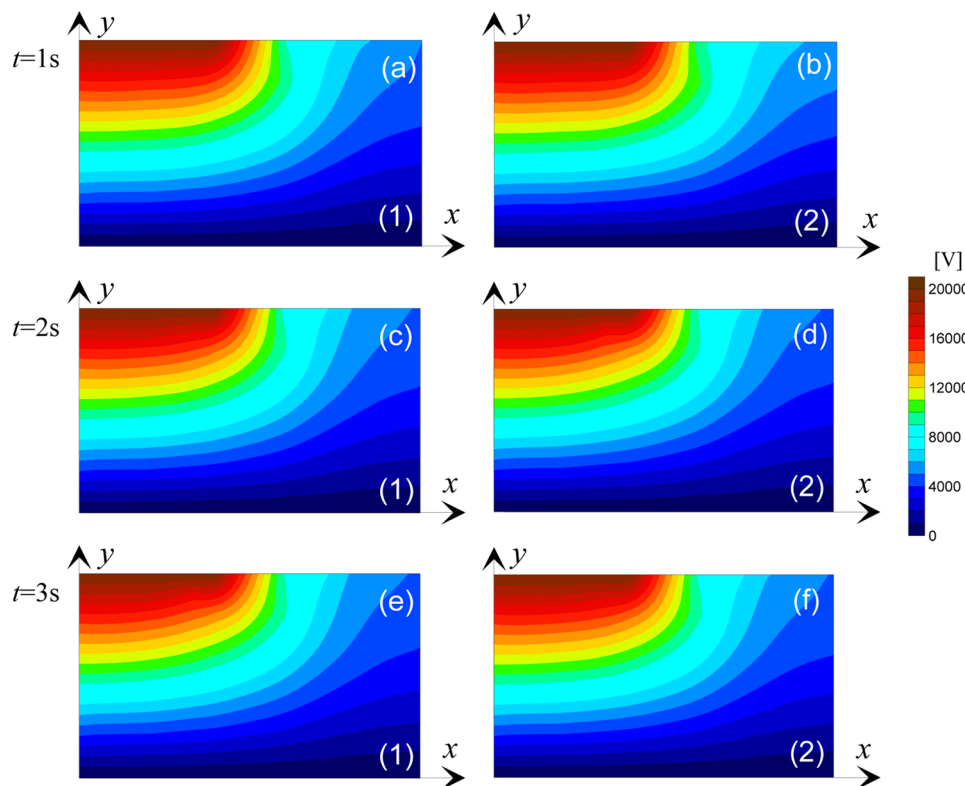


Figure 6. Electric potential field, expressed in volt, plotted in the undeformed polymeric body at the time instant $t = 1$ s for case 1 (slow kinetics, (1), a) and for case 2 (fast kinetics, (2), b). Corresponding electric potential field at the time instant $t = 2$ s (slow (c) and fast kinetics (d)) and 3 s (slow (e) and fast kinetics (f)). The maps are plotted only for the grey filled region of the specimen of Fig. 4a.

fraction of static cross-links ($f_c = 0.1$) assumed for the present problem.

In Figure 6, the potential field in the material is depicted at the time $t = 1, 2$, and 3 s; the distribution of the electric potential in the material (represented for sake of simplifying the comparison in the undeformed reference configuration) is slightly affected by the micromechanical remodeling of the material at $t = 1$ s, while a slight difference can be observed from Figure 6(c) and (d) related to cases 1 and 2 at $t = 2$ s, due to the greater deformation occurred in the material due to

the fast kinetics of case 2. No noteworthy differences can be appreciated for the later time instant $t = 3$ s for both cases 1 and 2, since the material has had enough time to rearrange its microstructure irrespectively of the kinetics.

In Figure 7, the stress fields in the material are depicted at time $t = 2$ s; the fastest internal relaxation of the material for case (2) gives rise to a lower stress values because of the greater ability of the polymeric network to reset at the nanoscale level to its initial free stress state.

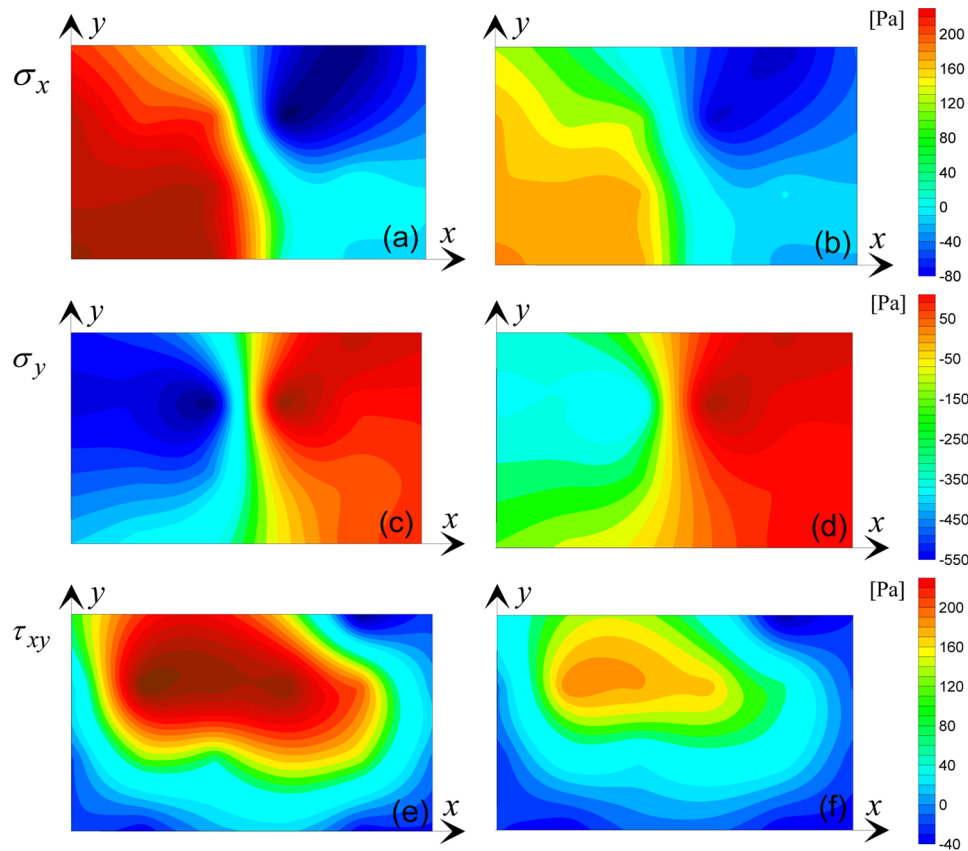


Figure 7. Cauchy stress field plotted in the undeformed polymeric body at the time $t = 2$ s for the case 1 (slow kinetics, (1), a, c, e) and for case 2 (fast kinetics, (2), b, d, f). Mechanical stress σ_x (a, b), σ_y (c, d), and shear stress τ_{xy} (e, f) (Pa) in the same instant (the maps are plotted only for gray filled region of the specimen, Figure 4(a)).

In fact, the stress field is significantly affected by the kinetics of the material and higher stress values arise in the body when a slow kinetic is considered. For the sake of simplicity, in Figure 7(a) to (f), the mechanical Cauchy stresses σ_x , σ_y , and τ_{xy} are represented on the undeformed configuration for the slow kinetic case 1 (left column) and for the fast kinetic case 2 (right column).

Cantilever beam actuator

As recalled in the introduction, dielectric elastomers are typically used as actuators in a wide range of applications; under a sufficiently strong electric field, their mechanical response is induced by the so-called Maxwell effect which is responsible for the material deformation. In the present example the actuator is represented by a slender beam, clamped at its left extremity, with a length equal to $L = 50$ mm, a width of 4 mm, and a thickness $w = 1$ mm; it is composed by two layers made of electrostrictive polyurethane (PU, assumed to have a relative electric permittivity $\epsilon_r = 10$), each one with a thickness of 0.5 mm. The compliant electrodes are properly arranged in the beam in order

to deform the upper part of the beam (Figure 8) (Ask et al., 2012a). The beam is discretized by adopting a regular mesh made of 50×4 ($L \times w$) bilinear quadrilateral elements, assumed to be in a plane stress state with respect to the y direction.

An electric potential difference $\Delta\Phi(t)$ is applied between the two electrodes; the effect induced by the deformation of the electrically stressed region of the element entails a downward bending of the beam due to the elongation of the beam's upper layer. The electric potential is made to vary according to the relation $\Delta\Phi(t) = \Delta\Phi_0 \cdot f(t)$, where $\Delta\Phi_0 = 5$ kV and the time function $f(t) = 2t$ for $0 \leq t \leq 0.5$ s, that is, a potential rate of 10 kV/s is applied.

The numerical integration of the electromechanical governing equations is performed by adopting a time step size equal to $\Delta t = 10^{-2}$ s during the electric potential increasing phase. Results obtained by the present model are compared with those provided in the literature (Ask et al., 2012a).

The viscoelastic behavior of the material is modeled by assuming a fraction of the total polymer's cross-links to be able to rearrange in time $f_d = 1 - f_c = 0.8$, the rearrangement kinetic is assumed to be governed by the

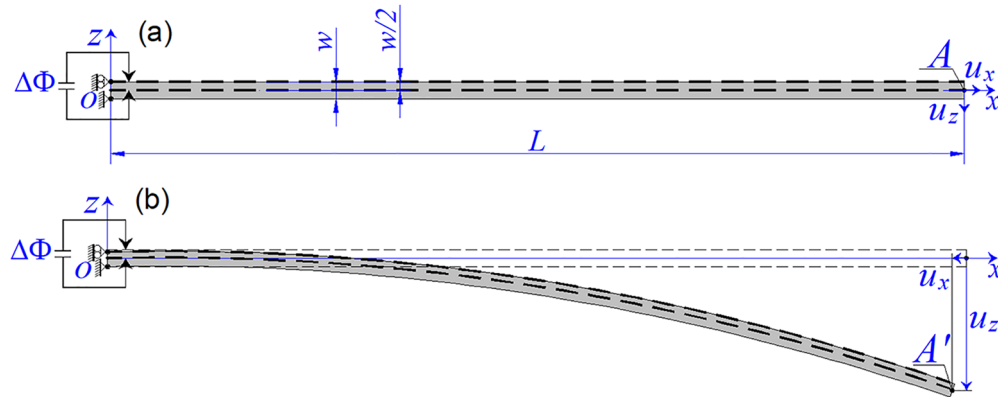


Figure 8. Beam-like actuator clamped at one extremity. The electrodes arrangement is shown by dashed lines placed on the top and along the midline of the beam (a). Scheme of the FE deformed configuration due to the application of the electric potential $\Delta\Phi$ (b).

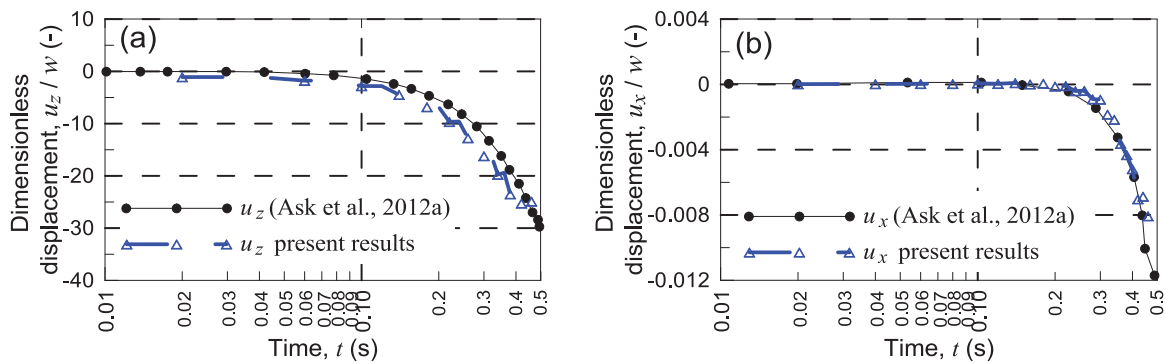


Figure 9. Dimensionless vertical (a) and horizontal (b) displacement of the beam-like actuator's tip (point A, see Figure 8(a)) compared with literature results in Ask et al. (2012a).

exchange rates $k_A = 25$, $k_D = 100$, while the adopted initial elastic modulus and Poisson's ratio are, according to Ask et al. (2012a), equal to $E_0 = 0.02$ MPa and $\nu = 0.48$, respectively.

Figure 9 shows the dimensionless vertical and horizontal displacements of the point A placed at the beam's tip versus time. The general trend of the downward and backward motion displayed by point A, obtained through the numerical simulation based on the exchange bond evolution of the polymeric network, provides a behavior which is satisfactorily close to the literature results.

Conclusion

The time-dependent response of electroactive polymers has been considered in the present paper. The electro-mechanical coupled governing equations have been formulated by accounting for the viscoelastic behavior of the material, modeled through an internal evolution of the polymeric network, corresponding to a dynamic

nature of the chains' cross-links. The mentioned remodeling feature is characteristic of a class of recently developed materials known as vitrimers and has been used here as a simple and effective tool to deal with time-dependent mechanical behavior of elastomers under an electrically induced deformation.

The physical interpretation of the developed equations has been recalled, with a special attention paid to the dissipation contribution to the balance equations featuring the time-dependent viscous behavior of the polymeric material. The computational implementation of the theoretical approach has been finally presented and some numerical examples have been illustrated and discussed in order to underline the capability and reliability of the proposed approach for modeling the time-dependent response of electroactive polymers.


Declaration of conflicting interests

The author(s) declared no potential conflicts of interest with respect to the research, authorship, and/or publication of this article.

Funding

The author(s) received no financial support for the research, authorship, and/or publication of this article.

ORCID iD

Roberto Brighenti  <https://orcid.org/0000-0002-9273-0822>

References

- Ask A, Denzer R, Menzel A, et al. (2013) Inverse-motion-based form finding for quasi-incompressible finite electroelasticity. *International Journal of Numerical Methods in Engineering* 94: 554–572.
- Ask A, Menzel A and Ristinmaa M (2012a) Electrostriction in electro-viscoelastic polymers. *Mechanics of Materials* 50: 9–21.
- Ask A, Menzel A and Ristinmaa M (2012b) Phenomenological modeling of viscous electrostrictive polymers. *International Journal of Non-Linear Mechanics* 47: 156–165.
- Ask A, Menzel A and Ristinmaa M (2015) Modelling of viscoelastic dielectric elastomers with deformation dependent electric properties. *Procedia IUTAM* 12: 134–144.
- Beatty MF and Stalnaker DO (1986) The poisson function of finite elasticity. *Journal of Applied Mechanics* 53: 807–813.
- Bergström JS and Boyce MC (2016) Constitutive modeling of the large strain time-dependent behavior of elastomers. *Journal of the Mechanics and Physics of Solids* 46: 931–954.
- Brighenti R and Vernerey FJ (2017) A simple statistical approach to model the time-dependent response of polymers with reversible cross-links. *Composites Part B: Engineering* 115: 257–265.
- Büschel A, Klinkel S and Wagner W (2013) Dielectric elastomers—numerical modelling of non-linear visco-electroelasticity. *International Journal of Numerical Methods in Engineering* 93: 834–856.
- Bustamante R, Dorfmann A and Ogden RW (2008) On variational formulations in nonlinear magnetoelastostatics. *Mathematics and Mechanics of Solids* 13: 725–745.
- Bustamante R, Dorfmann A and Ogden RW (2009) Nonlinear electroelastostatics: a variational framework. *Zeitschrift für angewandte Mathematik und Physik* 60: 154–177.
- Candau N, Laghmach R, Chazeau L, et al. (2014) Strain-induced crystallization of natural rubber and cross-link densities heterogeneities. *Macromolecules* 47(16): 5815–5824.
- Carpi F, De Rossi D, Kornbluh R, et al. (eds) (2008) *Dielectric elastomers as electromechanical transducers. fundamentals, materials, devices, models and applications of an emerging electroactive polymer technology*. Amsterdam: Elsevier.
- Cohen N, Menzel A and De Botton G (2016) Towards a physics-based multiscale modelling of the electro-mechanical coupling in electro-active polymers. *Proceedings of the Royal Society of London. Series A, Mathematical, Physical and Engineering Sciences* 472(2186): 20150462.
- Doi M (2013) *Soft Matter Physics*. Oxford: Oxford University Press.
- Dorfmann A and Ogden RW (2005) Nonlinear electroelasticity. *Acta Mechanica* 174: 167–183.
- Dorfmann A and Ogden RW (2012) Nonlinear electro- and magneto-elastic interactions. In: Merodio J and Saccomandi G (eds) *Continuum Mechanics, Encyclopedia of Physical Sciences, Engineering and Technology Resources*. Oxford: Encyclopedia of Life Support Systems (EOLSS), UNESCO-EOLSS, EPLSS Publishers, pp. 41–111.
- Dorfmann L and Ogden RW (2014) *Nonlinear Theory of Electroelastic and Magnetoelastic Interactions*. New York: Springer.
- Drozdov AD (1999) A constitutive model in finite thermoviscoelasticity based on the concept of transient networks. *Acta Mechanica* 133: 13–37.
- Flory PJ (1953) *Principles of Polymer Chemistry*. Menasha, WI: George Banta Publishing Company.
- Flory PJ (1989) *Statistical Mechanics of Chain Molecules*. Cincinnati, OH: Hanser-Gardner.
- Fricker HS (1973) On the theory of stress relaxation by cross-link reorganization. *Proceedings of the Royal Society of London. Series A, Mathematical, Physical and Engineering Sciences* 335: 289–300.
- Haldar K, Kiefer B and Menzel A (2016) Finite element simulation of rate-dependent magneto-active polymer response. *Smart Materials and Structures* 25: 104003.
- Jurowska A and Jurowski K (2015) Vitrimers—the miracle polymer materials combining the properties of glass and plastic? *Chemik* 69(7): 389–394.
- Kuhn W (1946) Dependence of the average transversal on the longitudinal dimensions of statistical coils formed by chain molecules. *Journal of Polymer Science Part A* 1: 380–388.
- Kuhn W and Grün F (1946) Statistical behavior of the single chain molecule and its relation to the statistical behavior of assemblies consisting of many chain molecules. *Journal of Polymer Science Part A* 1(3): 183–199.
- Lavoie SR, Long R and Tang T (2016) A rate-dependent damage model for elastomers at large strain. *Extreme Mechanics Letters* 8: 114–124.
- Meng F, Pritchard RH and Terentjev EM (2016) Stress relaxation, dynamics, and plasticity of transient polymer networks. *Macromolecules* 49(7): 2843–2852.
- Menzel A and Waffenschmidt T (2009) A microsphere-based remodelling formulation for anisotropic biological tissues. *Proceedings of the Royal Society of London. Series A, Mathematical, Physical and Engineering Sciences* 367: 3499–3523.
- Oldroyd J (1950) On the formulation of rheological equations of state. *Proceedings of the Royal Society of London. Series A, Mathematical, Physical and Engineering Sciences* 200(1063): 523–541.
- Orlandini E and Whittington SG (2016) Statistical mechanics of polymers subject to a force. *Journal of Physics A: Mathematical and Theoretical* 49(34): 343001.
- Osswald TA and Rudolph N (2014) *Polymer Rheology: fundamentals and Applications*. Munich: Hanser Publishers.
- Pelrine RE, Kornbluh RD and Joseph JP (1998) Electrostriction of polymer dielectrics with compliant electrodes as a means of actuation. *Sensors and Actuators A: Physical* 64: 77–85.
- Petiteau J-C, Verron E, Othman R, et al. (2013) Large strain rate-dependent response of elastomers at different strain rates: convolution integral vs. internal variable formulations. *Mechanics of Time-Dependent Materials* 17(3): 349–367.
- Rasmussen L (ed.) (2012) *Electroactivity in Polymeric Materials*. New York: Springer.

- Roland CM (2006) Mechanical behavior of rubber at high strain rates. *Rubber Chemistry and Technology* 79(3): 429–459.
- Smallenburg F, Leibler L and Sciortino F (2013) Patchy particle model for vitrimers. *Physical Review Letters* 111: 188002.
- Tagarielli V, Hildick-Smith R and Huber J (2012) Electro-mechanical properties and electrostriction response of a rubbery polymer for EAP applications. *International Journal of Solids and Structures* 49: 3409–3415.
- Thylander S, Menzel A and Ristinmaa M (2012) An electro-mechanically coupled micro-sphere framework: application the finite element analysis of electrostrictive polymers. *Smart Materials and Structures* 21: 094008.
- Thylander S, Menzel A and Ristinmaa M (2017) A non-affine electro-viscoelastic microsphere model for dielectric elastomers: application to VHB 4910 based actuators. *Journal of Intelligent Material Systems and Structures* 28: 627–639.
- Tiersten F (1971) On the nonlinear equations of thermoelectroelasticity. *International Journal of Engineering Science* 9: 587–604.
- Toupin R (1956) The elastic dielectric. *Journal of Rational Mechanics and Analysis* 5: 849–915.
- Treloar L (1975) *Physics of Rubber Elasticity*. 3rd ed. Oxford: Clarendon Press.
- Vernerey FJ, Long R and Brighenti R (2017) A statistically-based continuum theory for polymer with transient networks. *Journal of the Mechanics and Physics of Solids* 107: 1–20.
- Vu DK, Steinmann P and Possart G (2007) Numerical modeling of non-linear electroelasticity. *International Journal of Numerical Methods in Engineering* 70(6): 685–704.
- Wissler M and Mazza E (2007) Electromechanical coupling in dielectric elastomer actuators. *Sensors and Actuators A: Physical* 138: 384–393.
- Yang H, Yu K, Mu X, et al. (2015) A molecular dynamics study of bond exchange reactions in covalent adaptable networks. *Soft Matter* 11: 6305–6317.

Appendix I

Notation

$A = \mathcal{E} - T \cdot \eta(\mathbf{x}, t)$	Helmholtz free energy per unit volume
b	average length of the chain segments in the polymeric chain
\mathbf{b}	mechanical body force vector
\mathbf{b}_{e0}	forces per unit initial volume arising due to the electromechanical interaction
$\mathbf{B}_0, \mathbf{B}_t$	body force vector reference and deformed configuration domain of the body, respectively
$\partial \mathbf{B}_0, \partial \mathbf{B}_t$	boundary of the body in the reference and current configuration, respectively

c, c^t

$\mathbf{C}'_{Mech}, \mathbf{C}'_{MEI}, \mathbf{C}'_{EIM}, \mathbf{C}'_{EI}$

\mathbf{D}, \mathbf{d}

\mathcal{D}

\mathbf{E}, \mathbf{e}

\mathcal{E}

$\mathcal{E}_{Mech}(\boldsymbol{\mu}), \mathcal{E}_{MEI}(\mathbf{F}, \mathbf{E}), \mathcal{E}_{EI}(\mathbf{E})$

$f_c, f_d = 1 - f_c$

$\mathbf{F}, F_{ij} = \partial x_i / \partial X_j$

$\dot{\mathbf{F}}$

$J = \det \mathbf{F}$

k_B

k_A, k_D

$\mathbf{L} = \dot{\mathbf{F}}\mathbf{F}^{-1}$

n

$\mathbf{P}_{Mech}, \mathbf{P}_{MeI}$

\mathbf{P}, \mathbf{p}

$P_0(r), P(r)$

$\dot{\mathbf{q}}, \dot{\mathbf{Q}}$

concentration of the cross-links (attached chains) and maximum number of potentially mechanically active chains in the network per unit volume, respectively

purely mechanical, mechanical–electric, electric–mechanical, and purely electric tangent tensors of the electromechanical coupled material problem

vector of electric displacements in the reference and in the deformed configuration, respectively

internal energy dissipated by the material

electric field in the reference and in the current configuration, respectively

internal energy per unit volume

Mechanical, electro-mechanical and purely electrical contribution to the energy of the material per unit volume, respectively

volume fraction of the static and of the dynamic network in the polymer, respectively

macroscopic deformation gradient tensor

rate of macroscopic deformation gradient tensor

volumetric deformation

Boltzmann's constant

activation and deactivation rates, respectively

velocity gradient in the current (spatial) configuration

number of polymer chains' segments

first Piola–Kirchhoff mechanical stress tensor and electromechanical one, respectively

polarization vector in the reference and in the current configuration, respectively

probability function (normalized distribution) of the polymer chains' end-to-end distance in the stress-free reference state and in a generic one, respectively

rates of heat flux through the boundary and heat produced in the unit volume, respectively

$\mathbf{r}, r = \mathbf{r} , \dot{\mathbf{r}}$	end-to-end vector, its modulus, and time derivative for a single polymer chain, respectively	$\boldsymbol{\mu}$ $\vartheta(\mathbf{X}, t)$ $\rho_0 = \rho J$	distribution tensor deformation function referential mass density and its relation to the spatial mass density ρ
\mathbf{S}	symmetric part of the spatial velocity gradient tensor \mathbf{L}		
\mathbf{T}	total Piola stress tensor accounting for the mechanical and electro-elastic coupling	$\boldsymbol{\sigma}$ $\boldsymbol{\tau}$	Cauchy stress tensor total Cauchy stress tensor accounting for the mechanical and electro-elastic coupling
T	absolute temperature		distribution of the chains' end-to-end vector \mathbf{r} density in the initial stress-free state and in a generic time instant, respectively
$\mathbf{T}_{Mech}, \mathbf{T}_{Mel}$	vectors of the purely mechanical and of the electromechanical traction forces applied to the unconstrained portion of the boundary, respectively	$\varphi_0(\mathbf{r}), \varphi(\mathbf{r}, t)$	electric potential energy stored in the polymer for a given distribution of the end-to-end vector distance \mathbf{r}
\mathbf{X}, \mathbf{x}	position vector in the initial and in the current configuration, respectively	$\Phi(\mathbf{x}, t)$ $\psi(\mathbf{r})$	energy stored in a single chain having an end-to-end vector distance \mathbf{r}
$\varepsilon_0, \varepsilon_r$	electric permittivity of the free space and relative electric permittivity of the material, respectively	$\psi_c(\mathbf{r})$	augmented free energy of the material
$\eta(\mathbf{x}, t)$	entropy per unit volume of material	$\Psi(\mathbf{F}, \mathbf{E})$	